THERMODYNAMICAL BUDGETS OF AN EXPLICITELY SIMULATED DEEP CONVECTIVE CLOUD SYSTEM

Françoise GUICHARD[1], Jean-Philippe LAFORE[1] and Jean-Luc REDELSPERGER[1]

Centre National de Recherches Météorologiques (Météo-France and CNRS), Toulouse, FRANCE

1. INTRODUCTION

Representation of cumulus convection constitutes a critical point for large scale modelling. Numerous studies have stressed the sensitivity of large scale dynamics to the convection scheme that is used (Lindzen, 1990, Slingo *et al.*1994).

The present study aims to investigate the thermodynamical impact of an oceanic tropical cloud sytem simulated with a Cloud Resolving Model (CRM). Thermodynamical budgets are analysed, and some statistic properties are retrieved and discussed.

2. THE CONVECTIVE CLOUD SYSTEM

We focus on a cloud system observed on 17 February 1993 in the TOGA-COARE region (Fig. 1), formed of two convective lines, oriented approximatively parallel to the low level shear, with a life cycle of a few hours.

The simulation is performed in three-dimensions, with the CRM of Redelsperger and Sommeria (1986), over a spatial domain of 90(x).90(y).20(z) km^2. Ice phase processes (Caniaux *et al.*, 1994) as well as radiative effects (Morcrette 1991 - see Guichard *et al.*1996 for their implementation) are treated. The model starts with homogeneous conditions corresponding to the meteorological sounding, and cyclic

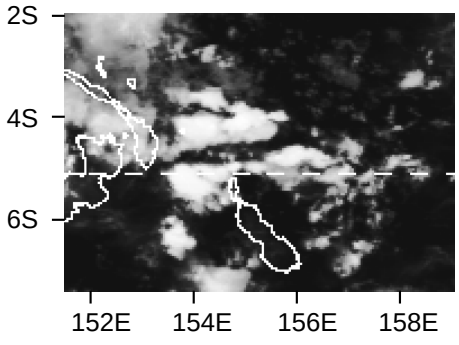

Figure 1: *IR satellite picture derived from the satellite GMS-4, at 21h45 UTC.*

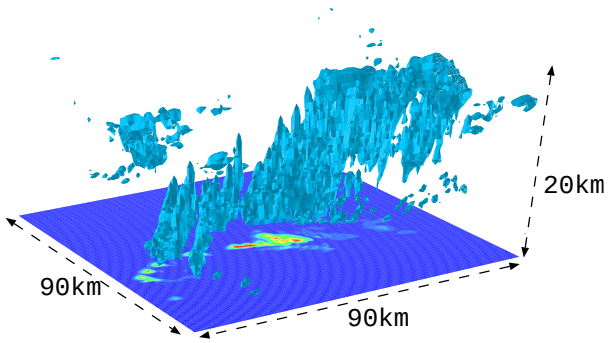

Figure 2: *Instantaneous field of simulated clouds and surface precipitation - isosurfaces (0.32g.kg^{-1}) of the sum of hydrometeors (cloud and precipitating liquid water, ice crystals, aggregates and graupel)*

lateral boundary conditions are used. No large scale ascent is prescribed in the simulation, as there is no evidence of such forcings from observations.

Additional information on this case (observations and conditions of simulation) can be found in Jabouille *et al.*(1996) and Redelsperger *et al.*(1995). As observed by Doppler radars, a convective line develops parallel to the low level shear after a few hours. An instantaneous 3D view (Fig. 2) illustrates the simulated convective system, formed of an ensemble of different cloud types, at different stage of their life cycle. Shallow clouds, deep growing cells as well as ice anvils are simultaneously present.

3. HEAT AND MOISTURE BUDGETS

Fig. 3 shows thermodynamical budgets derived from equations of the model for potential temperature θ and water vapour q_v, horizontally and temporally averaged over the whole domain and the 2 hours of deep convection (multiplied by the Exner function π and $-L/c_p$ respectively, with L the latent heat of vaporisation).

In the present case, without large scale convergence, eulerian evolutions of θ and q_v are due to the

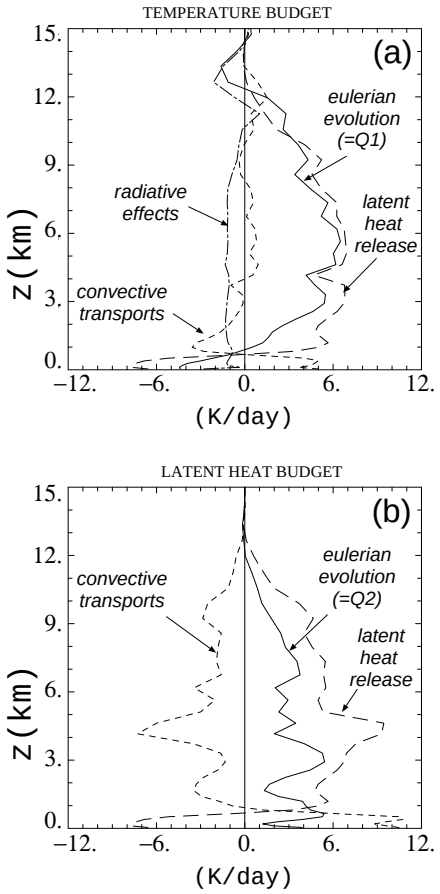

Figure 3: *Budgets of temperature (a) and latent heat (b) horizontally averaged over the whole domain and temporally over the 2 hours of deep convection*

sum of latent heat release, divergence of vertical convective fluxes (subgrid and resolved), and radiative effects (for θ only). Thus, eulerian evolution profiles correspond directly to apparent heat source Q_1 and apparent moisture sink Q_2 as defined at the large scale.

In Fig. 3a, the latent heat release appears to be the dominant process, explaining the average heating of the domain, whereas terms related to radiation and convective transport remain smaller, except below 2 km (where there is large convective transport) and at the cloud top (where large radiative effects occur). Finally, the maximum of Q_1, located around 6 km, is in agreement with observational results obtained during the COARE experiment (Lin and Johnson, 1996).

For water vapour (Fig. 3b), both latent heat release and convective eddy transports are important and in opposing. Latent heat release dries the atmosphere above 1 km and moistens it below through raindrops evaporation, whereas convective transports bring water vapour upwards.

The resulting Q_2 corresponds to a drying over the whole column, with a complex vertical structure. This particular shape differs somehow from the clas-

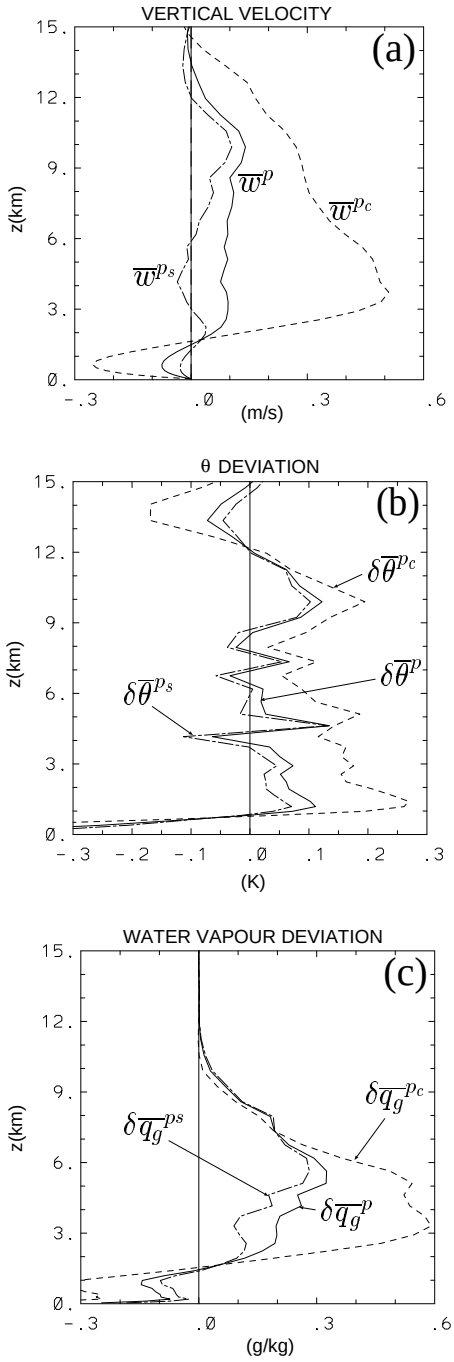

Figure 4: *For the precipitating system P, its convective and stratiform parts P_C and P_S: vertical profiles of (a) vertical velocities and deviations from the average over the whole domain of (b) potential temperature θ - $\overline{\delta\alpha}^k = \overline{\alpha}^k - \overline{\alpha}^T$*

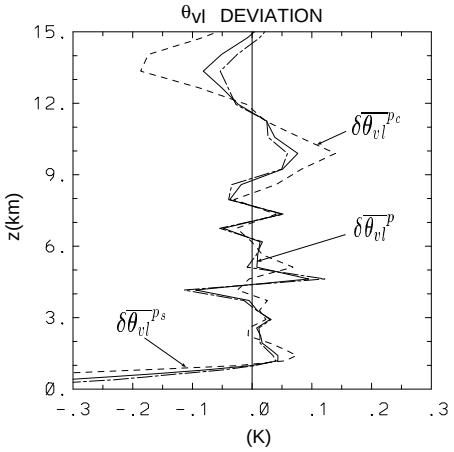

Figure 5: *Same as Fig.4b for deviations of liquid and solid virtual potential temperature θ_{vl}.*

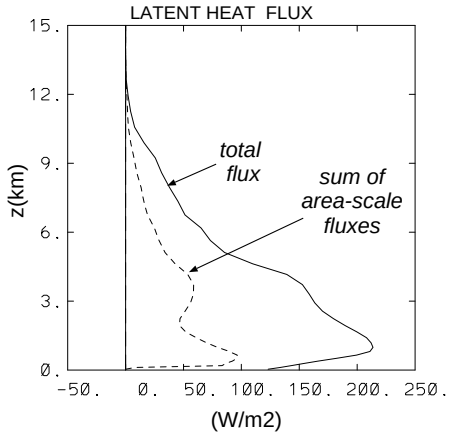

Figure 6: *Vertical fluxes of latent heat: total convective flux (solid line) and the sum of 'area-scale' fluxes (dashed line) - the sum of 'area-scale' fluxes is the sum of mean fluxes in updrafts and downdrafts for each of the 6 defined internal areas (see text).*

sical double peak structure, observed for large convective systems such as squall lines (e.g. Johnson 1984, Lafore *et al.*1988, Caniaux *et al.*1994). In particular, the second high peak is not strongly marked, and a third peak is observed at low level, in addition to the 3 km peak. Differences in the structure of the convective line could explain these differences. In particular, the stratiform part of the system, which is not very developped, can explain differences in high levels, and the presence of shallow convection those noted at low levels.

4. STATISTICAL PROPERTIES OF THE CLOUD SYSTEM

The precipitating system P is defined as the ensemble of columns where the integrated precipitating cloud water content is greater than 1 kg m^{-2}, over the 2 hours of deep convection. P is further split into convective and stratiform parts P_C and P_S, using criteria similar to Tao *et al.*(1989) for the convective area.

The area of convective precipitation is responsible for about 80% of the total latent heat release, although it covers only 4% of the total domain. The precipitating system P extends more widely (20%), whereas the remaining non-precipitating 80% consists of columns of clear sky, with embedded non precipitating shallow and convectively generated anvil clouds. Above the lower layers, air parcels ascend in P with a maximum of velocity located arround 10 km (Fig. 4a). It is higher than the one in P_C, due to stratiform clouds activity. The vertical velocity profile in the convective part of the system shows a typical structure, with strong convective downdrafts below 2 km and a maximum of 0.5m.s^{-1} at 3 km.

Above 1 km, the precipitating system is actually warmer than the environment, except locally, arround the isothermal 0°C in particular (Fig. 4b). However, the temperature excess does not even reach 0.3 K in the convective precipitation area.

These features agree with aircraft data analyses which stress surprisingly weak vertical velocities and temperature excesses in oceanic tropical convective cells (Lucas *et al.*1994).

Water vapour deviations in the precipitating system tend to increase the small buoyancy excess given by potential temperature deviations (Fig. 4c). They are correlated to vertical velocity, moister air is found is ascending layers and dryer air in subsidence layers.

In considering θ_{vl}, the liquid and solid virtual potential temperature, which takes into account water loading, in-cloud θ_{vl} deviations are still weaker (compare Fig. 4b with Fig. 5). The system shows an equilibrium of mass, due firstly to very small temperature deviations, and further reinforced by water in all its phases. The impact of water loading in reducing buoyancy, and thus vertical velocity, is stressed once again in the present simulation. The main point is that this result gives a relation between thermodynamics and microphysics in and outside clouds, this could be interesting for a convection scheme.

5. CONVECTIVE TRANSPORTS SCALE

Moisture budget (Fig. 3b) shows that convective vertical transport has a strong impact on water vapour distribution, so that a parameterization should be able to estimate it correctly.

Several internal areas i are defined, and we analyse whether the total convective transport could be explained as the sum of the different 'area-scale' transports. The total convective flux is decomposed as follow:

$$\rho\,\overline{q_v w}^T \;=\; \sum_i \rho\,\sigma_i\,\overline{w}^i\,\overline{q}_v{}^i \;+\; \sum_i \rho\,\sigma_i\,\overline{w''_i q''_{v\,i}}^i$$

$\overline{\alpha}^T$ and $\overline{\alpha}^i$ are the averages of α over the total domain and the area i respectively, ${\alpha''}_i = \alpha - \overline{\alpha}^i$, σ_i is the occupation rate of area i and ρ the air density. With this decomposition, it is possible to determine whether fluxes occur at the areas scale (first term of the right hand side), or at an even smaller scale (second term of the right hand side).

In each internal area i, the vertical flux of water vapour is well estimated by the average vertical flux deduced from average water vapour and vertical velocity fields in these areas ($\overline{wq_v}^i \approx \overline{w}^i \overline{q_v}^i$). However, strong compensations occur between vertical transports in the different areas of the domain, so that the total transport is a residual of them.

Six basic internal areas are retained here: the areas of surface convective and stratiform precipitation, the part of the cloud system where precipitation does not reach the ground, the areas of shallow and anvil clouds and clear sky columns (criteria are defined in Guichard 1995). Then, we further distinguish the updraft and downdraft parts of each area. The contribution of each of the twelve areas to the total flux is computed and separated into an average area-scale and a sub-area scale contribution. Results are presented for a 2 hour temporal average, but the conclusion is the same for shorter periods (Fig. 6).

In considering the contributions of both average updrafts and downdrafts in each internal area, it is possible to retrieve only between 1/3 and 1/2 of the total flux (the retrieval is even worse for sensible heat flux). Thus, knowledge of mean vertical properties of internal areas is not reliable, it leads to a large underestimation of the convective flux. Sub-areas draft fluxes are necessary in order to get a good estimation of the total flux. This raises a delicate problem in terms of parameterization.

6. SUMMARY

A convective line has been explicitely simulated. It develops along the shear direction in low levels, as observed during the COARE experiment. Its thermodynamical budgets and statistical properties have been analysed and discussed. In particular, this study brings out the fact that the simulated atmospheric column exhibits an equilibrium of mass, and that convective transports occur on a very fine scale. Additional work is necessary to validate the simulation results with COARE observations (Doppler radar data), and other convective systems have to be similarly analysed for evaluating the sensitivity of cloud statistic properties.

REFERENCES

Caniaux, G., J.-L Redelsperger and J.-P. Lafore, 1994: A numerical study of the stratiform region of a fast-moving squall line. Part I: general description and water and heat budgets. *J. Atmos. Sci.*, **51**, 2046-2074.

Guichard, F., J.-L Redelsperger and J.-P. Lafore, 1994: The behaviour of a cloud ensemble in response to external forcings, *Quart. J. Roy. Meteor. Soc.*, accepted.

Guichard, F, 1995: Impact d'un ensemble de nuages sur l'environnement de plus grande échelle, vu par un modèle de convection nugeuse explicite (cas GATE et TOGA-COARE). cloud ensemble in response to external forcings, PhD thesis, Institut National Polytechnique de Toulouse, 197 pp.

Jabouille, P., J.-L. Redelsperger and J.-P. Lafore, 1996: Modification of surface fluxes by atmospheric convection as viewed from numerical simulation. *Mon. Wea. Rev.*, **124**, 816-837.

Johnson, R.H., 1984: Partitioning tropical heat and moisture budgets into cumulus and mesoscale components: implications for cumulus parameterization, *Mon. Wea. Rev.*, **112**, 1590-1602.

Lafore, J.-P., J.-L.Redelsperger and G. Jaubert, 1988: Comparison between a three-dimensional simulation and doppler radar data of a tropical squall line: transport of mass, momentum, heat and moisture. *J. Atmos. Sci.*, **45**, 3483-3500.

Lin, X. and R.H. Johnson, 1996: heating, moistening and rainfall over the Western Pacific Warm Pool during TOGA COARE, *submitted to J. Atmos. Sci.*.

Lindzen, R. S., 1990: Some coolness concerning global warming. *Bull. Amer. Meteor. Soc.*, **71**, 288-299.

Lucas, C. and E.J. Zipser and M.A. LeMone, 1994: Vertical velocity in oceanic convection off tropical Australia. *J. Atmos. Sci.*, **51**, 3183-3193.

Morcrette, J.-J, 1991: Radiation and cloud radiative properties in the european centre for medium range weather forecasts forecasting system. *J. Geophys. Res.*, **96**, 9121-9132.

Redelsperger, J.-L., and G. Sommeria, 1986: Three-dimensional simulation of a convective storm: sensitivity studies on subgrid parametrisation and spatial resolution. *J. Atmos. Sci.*, **43**, 2619-2635.

Redelsperger, J.-L., P. Jabouille and J.-P. Lafore, 1995: Numerical studies of convective organization observed during TOGA-COARE, Proceedings of the 21st Conference on Hurricanes and Tropical Meteorology, paper 14B.6.

Slingo, J. M., M. Blackburn, A. K. Betts, R. Brugge, K. Hodges, B. J. Hoskins, M. J. Miller, L. Steenman-Clark and J. Thuburn, 1994: Mean climate and transience in the tropics of the UGAMP GCM: Sensitivity to convective parametrization. *Quart. J. R. Met. Soc.*, **120**, 881-922.

Tao, W.-K and J. Simpson, 1989: Modeling study of a tropical squall-type convective line. *J. Atmos. Sci.*, **46**, 177-202.